Figures and Figure Captions

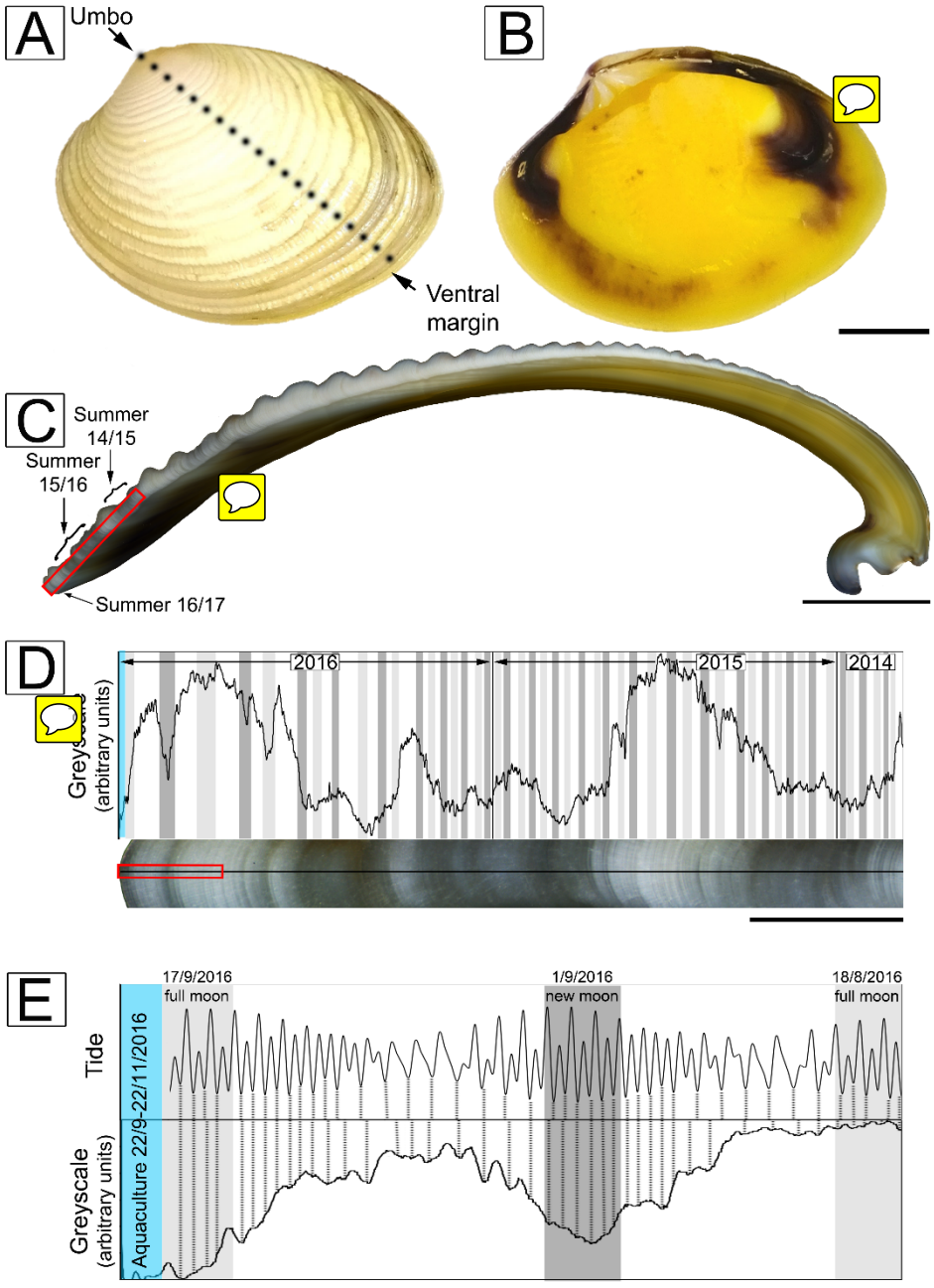

Figure 1: Outside (A) and inside (B) view of an unlabelled *K. rhytiphora* shell. Dashed black line in (A) indicates where the shell was sectioned. All cross-sections in this study are prepared as radial sections along the maximum growth axis unless otherwise specified. (C). Dark bands (arrows in C) are summer growth periods between lighter coloured winter periods and are magnified in D (red box in C) with a greyscale line profile. Distinct troughs in greyscale intensity correlate with 48 out of 50 spring tides in two

years from the collection site of the bivalves (full moon: light grey, new moon: dark grey) giving fortnightly growth resolution in this shell area. Greyscale line profiles (E) of the area marked by the red box in D shows the most recent shell growth increment in the wild (mid-August to mid-September 2016). In this part tides correlate with most shell increments (black dashed lines), while this correlation is lost after start of aquaculture (blue area). Blue area in D, E marks the aquaculture period with lower than normal growth rates. Scale bars are 10 mm (A-B), 5 mm (C), 1 mm (D), 0.1 mm (E).

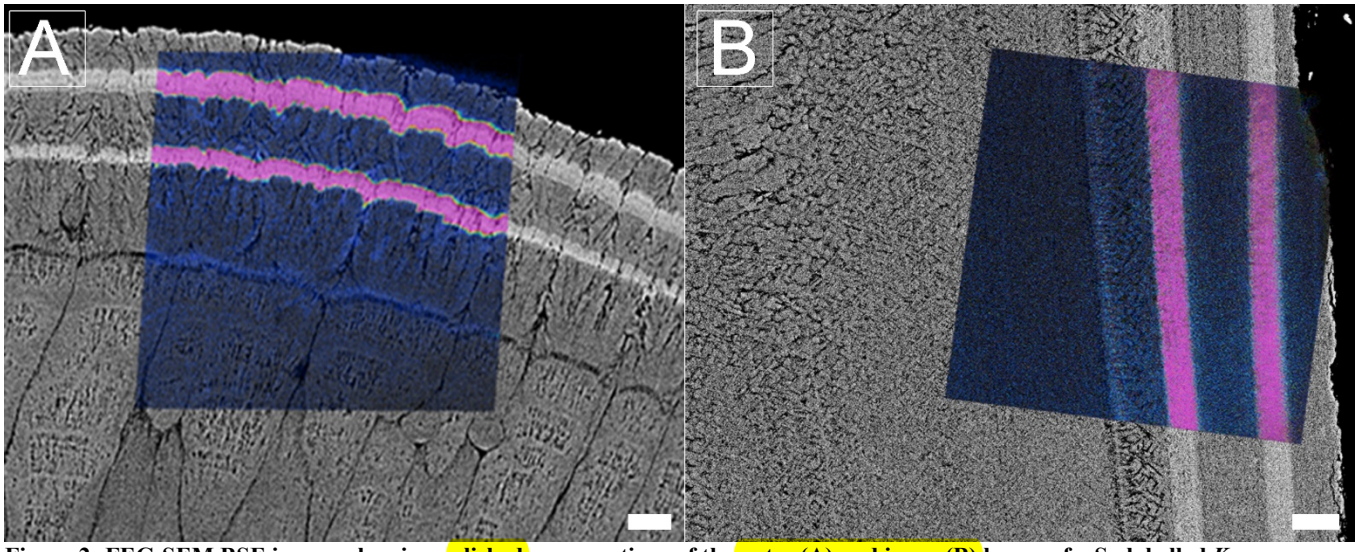

Figure 2: FEG-SEM BSE images showing polished cross-sections of the outer (A) and inner (B) layers of a Sr-labelled *K. rhytiphora* shell (specimen ID: K2-06) overlain with NanoSIMS $^{88}Sr/^{40}Ca$ maps. Ambient seawater $^{88}Sr/^{40}Ca$ ratios are depicted in blue, while shell formed during Sr-enriched incubations are shown in pink. Scale bars are 10 µm.

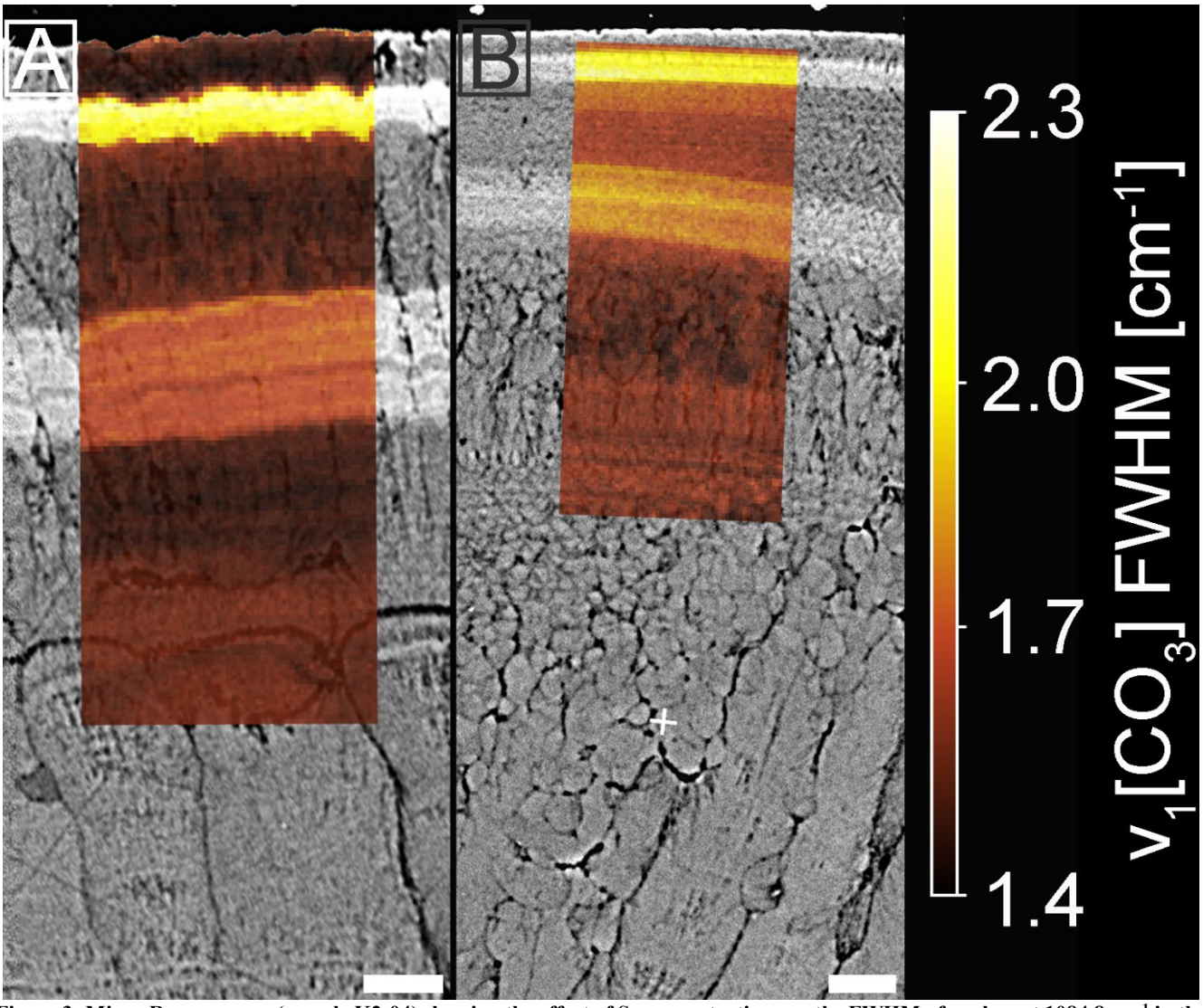

Figure 3: Micro-Raman maps (sample K2-04) showing the effect of Sr concentrations on the FWHM of peak ν_1 at 1084.8 cm^{-1} in the outer (A) and inner layer (B). Raman maps are overlain on BSE image. Bright grey-scale areas in the BSE images show elevated Sr-contents correlating with peak broadening (FWHM increase, see scale in cm^{-1}) in the labelled shell areas. For Micro-Raman maps of peak shifts see Fig. S2. All values are bandwidth corrected after Váczi (2014). Scale bars are 10 µm.

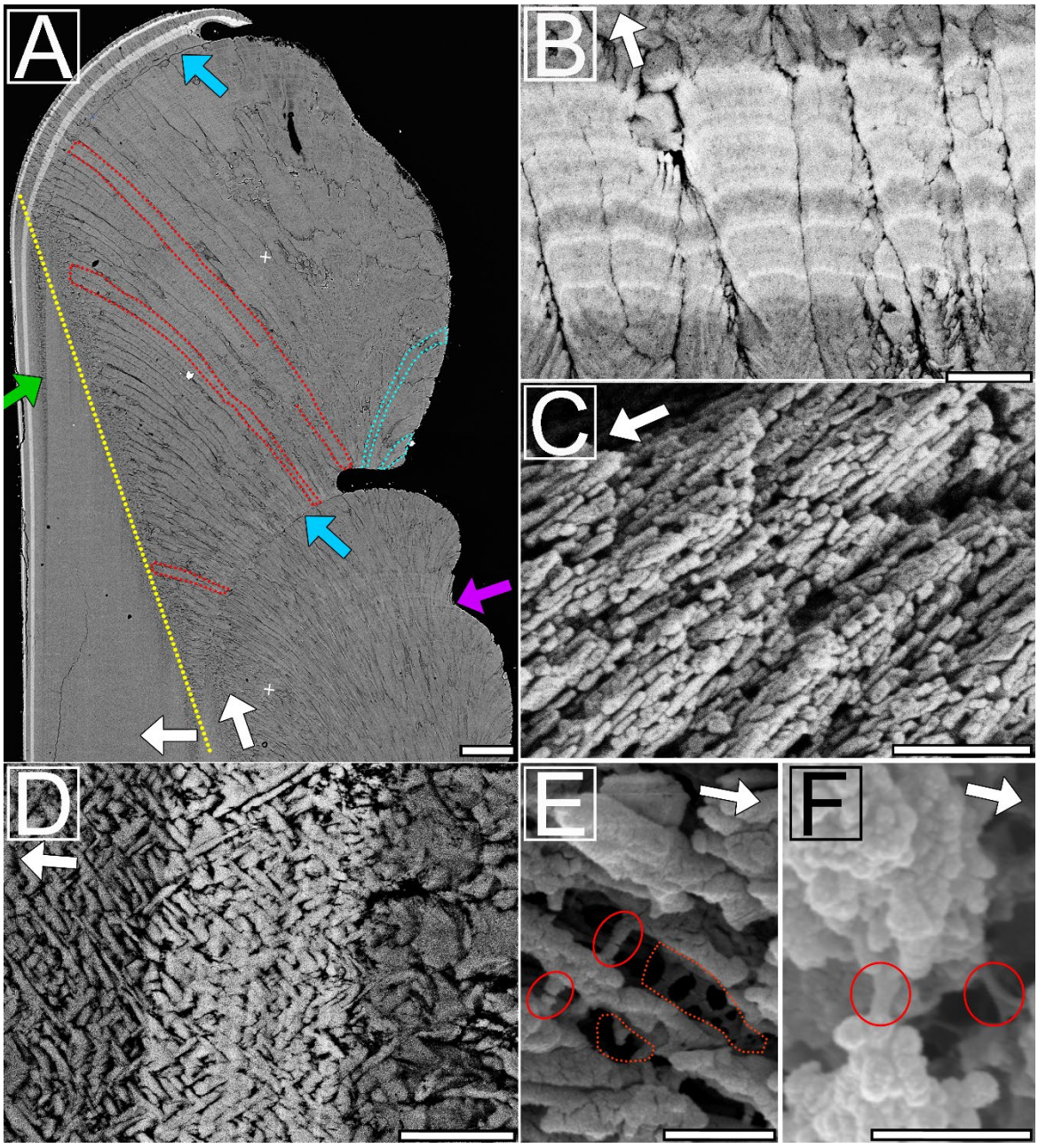

Figure 4: Backscattered images showing cross-sections along the maximum growth axis of Sr-labelled *K. rhytiphora* shells: (A) shows the ventral margin of the shell. First-order prisms in the prismatic outer layer bend inwards (red outlined) reach lengths of up to 700 µm with widths of 17 µm. Outward bending prisms (blue outlined) form the ridged surface ornamentation of the shell. Organic-rich growth checks are observed to occur directly at the end of a ridge feature (blue arrows), while not all ridge features are concluded by growth checks (purple arrow). The yellow dashed line marks boundary between inner and outer shell layers. Both Sr-labels show bright grayscales and follow the growth front of the shell. In the inner layer, the growth check continues as a prismatic

layer (green arrow). Strontium-labels within the outer layer (B) show first-order prisms to consist of radially arranged second-order prisms, which in turn consist of third-order prisms with their long axis parallel to each other, as seen in a broken piece of shell (C, Fig. S11). The inner, crossed acicular layer (D, BSE image) is composed of needle-like lamellae intersecting at an angle of ca. 82°. Etched specimens (E, F: SE images) reveal the nano-granular texture of the mineral phase as well as organic compounds with fibre (red circles) and sheet-like structures (dashed red lines) in the prismatic (E) and crossed acicular (F) layers. White arrows mark the general growth direction for each ultrastructure. For more details see Fig. S5-S8. Scale bars: 100 µm (A), 5 µm (B and D), and 500 nm (C, E and F).

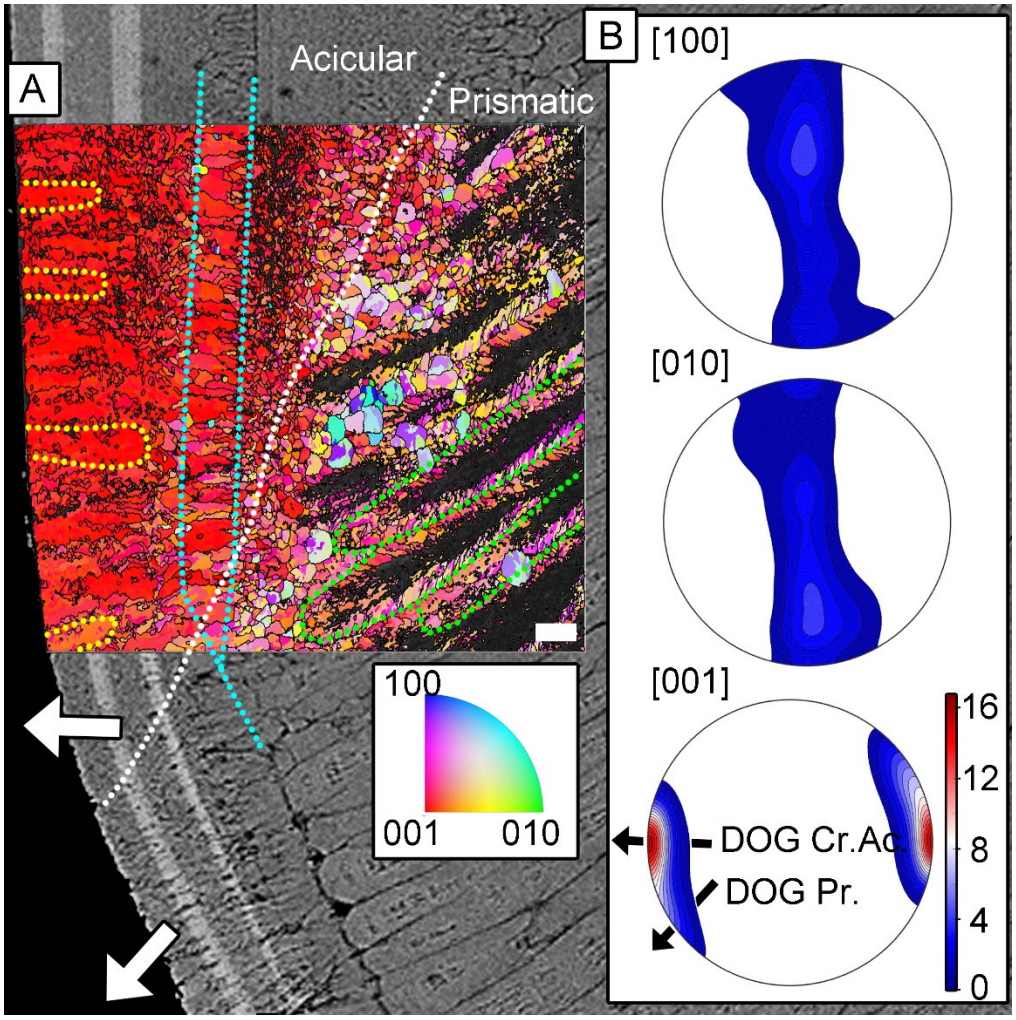

Fig. 5: Orientation map for aragonite (A) of a pulsed Sr-labelled K. rhytiphora shell (specimen ID: K2-11). Blue, green, and red represent the crystallographic a- [100], b- [010], and c-axes [001] of aragonite, respectively. The map is color-coded to show which crystallographic axis is aligned parallel to the growth direction of the shell-layers. The dotted white line indicates the boundary between inner and outer shell layers. The organic growth check in the outer structure that transitions into a thin prismatic layer in the inner layer is highlighted with light blue dotted lines. First-order prisms in the outer structure (some green outlined) have unindexed cores, while feathery arranged second-order prisms are visible at their rims. Individual lamellae of the inner layer form co-oriented stacks up to 17 µm in size (circled yellow). Pole figures (B) (lower hemisphere, equal area projection) show a strong clustering of [001] axes for both shell layers and coincides with the growth direction of the inner layer (DOG Cr.Ac.), but is at an angle relative to the growth direction of the outer layer (DOG Pr. In B). Crystallographic a- and b-axes are randomly distributed in the plane normal to the growth direction (i.e. containing the growth lines of the inner layer). Maximum density values of pole figures are color-coded according to scale bar with the [001] axes achieving 16.79 times uniform. Scale bar is 10 µm.

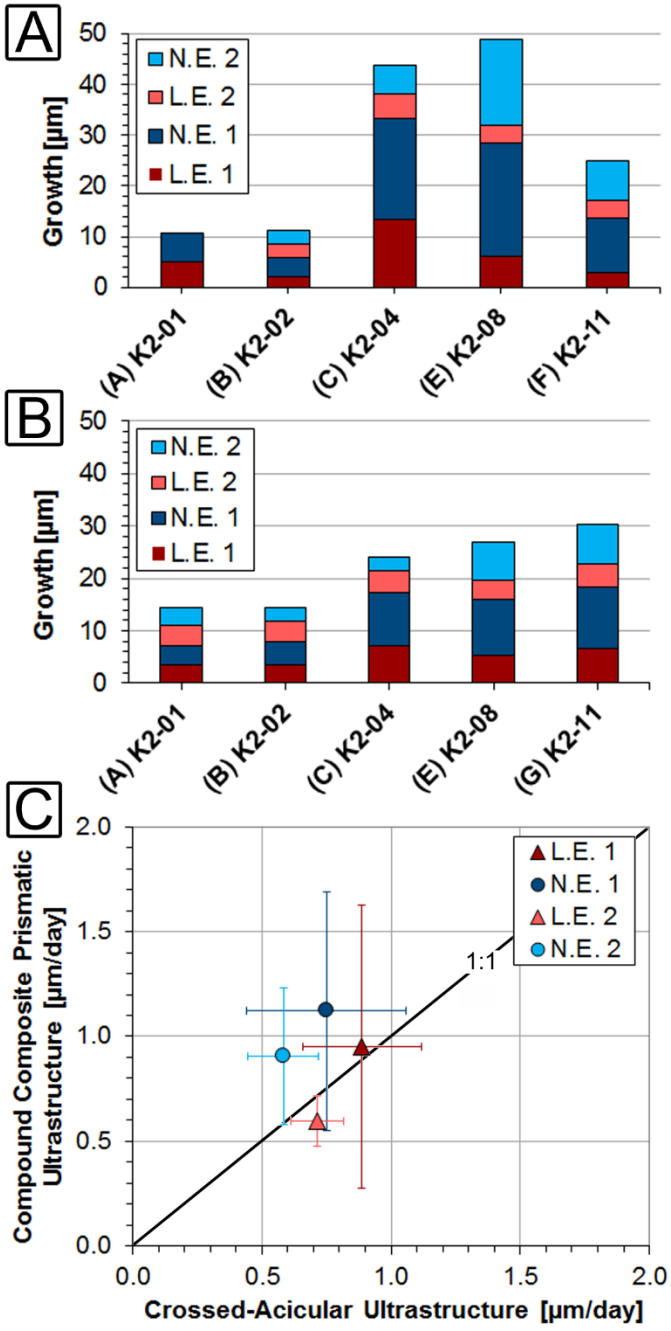

Figure: 6: Average growth of the outer compound composite prismatic (A) and inner crossed acicular layers (B) (Table 2). Distances were measured thrice at 5 different locations (Fig. S13, S14) along the axis of maximum growth using ImageJ. Growth rates agree well between labelling and ambient conditions and are within 1σ (C).

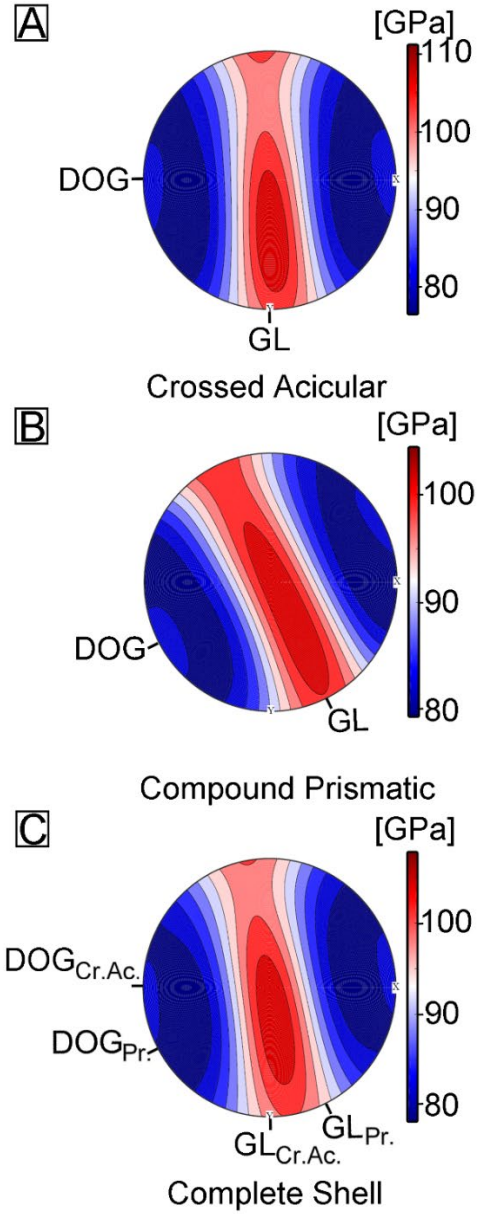

Figure 7: Young moduli (upper hemisphere and equal area projection), for the compound composite prismatic (A) and crossed acicular structure (B) as well as complete shell (C). Calculations were made with the Hill averaging scheme and used the aragonite single crystal elastic properties of Pavese et al. (1992) and the EBSD data collected for this study as inputs (Mainprice et al., 2011). For every section, the minimum force needed to induce a fracture coexists with the local direction of growth. The shell presents a plane of greater resistance (~20-25% increase) normal to the local direction of growth and is oriented parallel to the growth lines.

Tables:

Table 1: Geochemical composition of *K. rhytiphora* obtained from wavelength-dispersive X-ray spectrometry (WDS) electron probe micro analyser (EPMA) provided as wt.% ($g \cdot g^{-1}$) averages (Avg.) and standard deviations (Stdev.) for shell compositions grown under different conditions in the wild ("pre-aqua"), in aquaculture during labelling ("LE 1" and "LE 2"), and non-labelling ("pre-NE 1" and "NE 1") experiments.

			Na_2O	MgO	SO_3	Cl	CaO	SrO
Compound composite prismatic	**Pre-Aqua**	**Avg.**	**0.72**	**0.03**	**0.10**	**0.04**	**54.38**	**0.12**
	(n=5)	Stdev	0.06	0.02	0.04	0.01	0.20	0.03
	Pre-LE 1	**Avg.**	**0.57**	**0.04**	**0.14**	**0.04**	**54.73**	**0.13**
	(n=3)	Stdev	0.04	0.01	0.03	0.01	0.07	0.01
	LE 1	**Avg.**	**0.56**	**0.04**	**0.12**	**0.03**	**52.86**	**2.36**
	(n=3)	Stdev	0.04	0.01	0.02	0.01	0.09	0.07
	NE 1	**Avg.**	**0.41**	**0.03**	**0.17**	**0.03**	**54.72**	**0.31**
	(n=3)	Stdev	0.01	0.03	0.05	0.02	0.43	0.01
	LE 2	**Avg.**	**0.65**	**0.04**	**0.12**	**0.02**	**53.80**	**2.29**
	(n=3)	Stdev	0.04	0.01	0.03	0.01	0.15	0.02
Crossed Acicular*	**Pre-Aqua**	**Avg.**	**0.75**	**bdl**	**0.05**	**0.02**	**54.01**	**0.11**
	(n=5)	Stdev	0.09	-	0.06	0.01	0.06	0.04
	Pre-LE 1	**Avg.**	**0.77**	**bdl**	**0.05**	**0.02**	**53.76**	**0.10**
	(n=3)	Stdev	0.09	-	0.03	0.02	0.07	0.04
	LE 1	**Avg.**	**0.75**	**bdl**	**0.13**	**0.03**	**53.18**	**1.43**
	(n=3)	Stdev	0.09	-	0.07	0.01	0.06	0.04
	NE 1	**Avg.**	**0.72**	**0.03**	**0.20**	**0.02**	**54.52**	**0.15**
	(n=3)	Stdev	0.09	0.05	0.07	0.02	0.06	0.04
	Limits of Detection:		**0.05**	**0.02**	**0.04**	**0.01**	**0.04**	**0.02**

MnO (<0.025), BaO (<0.018), P_2O_5 (<0.028), K_2O (<0.017), and FeO (<0.020), were analyzed and always below detection limits (provided in brackets as wt.%). *LE2 and NE 2 in the crossed acicular ultrastructure were too close to the edge to be measured with confidence and are excluded.

Table 2: Average growth rates from pulsed Sr-labelling experiments. Full lists of all measurements in Tables S3, S4. Rates in italics in ambient conditions NE2 were deposited within 6 days, all other rates within 12 days. Daily growth rates over the experimental period are 0.85 and 0.73 µm for the outer and inner layer, respectively, resulting in a ~17 % higher growth rate for the outer layer.

Sample ID:	Structure:	LE 1 [µm/6d]	NE 1 [µm/12d]	LE 2 [µm/6d]	NE 2 [µm/6d] [µm/12d]	Total growth experimental period [µm/*30d*] or [µm/36d]	Daily growth experimental period [µm/d]
K2-01*	Outer	5.1 ± 0.6	5.7 ± 0.6	n.a.	n.a.	*10.8 ± 1.1*	0.66 ± 0.08
	Inner	3.5 ± 0.2	3.7 ± 0.3	4.0 ± 0.2	*3.3 ± 0.2*	*14.5 ± 0.9*	0.53 ± 0.03
K2-02	Outer	2.2 ± 0.4	3.7 ± 0.5	2.6 ± 0.5	*2.8 ± 0.3*	*11.3 ± 1.6*	0.39 ± 0.08
	Inner	3.6 ± 0.3	4.3 ± 0.3	3.9 ± 0.2	*2.6 ± 0.3*	*14.4 ± 1.1*	0.45 ± 0.05
K2-04	Outer	13.3 ± 0.9	20.0 ± 0.6	4.8 ± 0.7	*5.8 ± 0.8*	*43.9 ± 2.9*	1.41 ± 0.15
	Inner	7.0 ± 1.9	10.2 ± 1.0	4.3 ± 0.4	*2.6 ± 0.7*	*24.0 ± 3.9*	0.79 ± 0.17
K2-06	Outer	3.8 ± 1.2	10.5 ± 1.7	3.5 ± 0.7	12.4 ± 1.6	30.1 ± 1.3	0.78 ± 0.12
	Inner	6.0 ± 0.6	13.6 ± 0.6	5.5 ± 0.2	10.1 ± 0.4	35.1 ± 1.8	0.97 ± 0.05
K2-08	Outer	6.4 ± 1.8	22.3 ± 1.6	3.5 ± 0.9	16.9 ± 0.5	49.2 ± 1.2	1.23 ± 0.13
	Inner	5.2 ± 0.5	10.7 ± 0.3	3.7 ± 0.3	7.3 ± 0.3	26.9 ± 1.4	0.75 ± 0.08
K2-11	Outer	2.8 ± 0.7	10.8 ± 1.3	3.6 ± 0.9	7.7 ± 1.3	24.9 ± 4.2	0.65 ± 0.11
	Inner	6.7 ± 0.3	11.6 ± 0.2	4.4 ± 0.2	7.6 ± 0.3	30.3 ± 0.9	0.86 ± 0.02
	Av. Outer	**5.6 ± 0.9**	**12.2 ± 1.1**	**3.6 ± 0.7**	**9.1 ± 0.9**	**28.4 ± 2.1**	**0.85 ± 0.11**
	Av. Inner	**5.3 ± 0.6**	**9.0 ± 0.5**	**4.3 ± 0.3**	**5.6 ± 0.4**	**24.2 ± 1.7**	**0.73 ± 0.07**

*This individual did not show prismatic growth after NE1, while the crossed acicular structure kept growing.